Optimization of Tailoring of CuO_x Species of Silica Alumina Supported Catalysts for the Selective Catalytic Reduction of NO_x

Simona Bennici,[†] Antonella Gervasini,*[,†] Nicoletta Ravasio,[‡] and Federica Zaccheria[‡]

Dipartimento di Chimica Fisica ed Elettrochimica, Università degli Studi di Milano, Via Camillo Golgi n. 19, I-20133 Milano, Italy, and CNR Istituto ISTM, c/o Dipartimento di Chimica Inorganica, Metallorganica ed Analitica, Università degli Studi di Milano, Italy

Received: September 13, 2002; In Final Form: March 28, 2003

A series of CuO_x catalysts dispersed on $SiO_2-Al_2O_3$ support with a copper content from 0.2 to 12 wt % corresponding to 0.04−3.7 $atom_{Cu}\ nm^{-2}$ was prepared by chemisorption-hydrolysis method from copper solutions. The catalysts were characterized in their bulk (XRD, redox cycles with H_2 and O_2) and surface (N_2 adsorption, SEM, XPS, and DRS) properties. Copper species were found to be uniformly spread on the $SiO_2-Al_2O_3$ support as small aggregates both in the low and high copper loaded samples. Spectroscopic evidence agrees with Cu^{2+} presence in an axially distorted octahedral environment of O-containing ligands. At high copper loading, the existence of copper centers in closer interaction occurred forming structures of oxocations-like type. Temperature programmed reduction (TPR) experiments confirmed the presence of dispersed copper species which underwent complete reduction. Comparing the position and shape of two successive TPR profiles, carried out interposing an oxidation run (temperature programmed oxidation), it was found that the smallest CuO_x centers (<1 $atom_{Cu}\ nm^{-2}$) are characterized by low stability and high mobility. Increasing the copper content diminished the mobility of the CuO_x species, as larger CuO_x aggregates were formed. The selective catalytic reduction of NO_x with ethene in the presence of excess oxygen was studied in a flow apparatus at fixed reactant concentration (1500 ppm of NO_x and C_2H_4 and 15000 ppm of O_2) and contact time (8 g s $mmol^{-1}$), with an online FT-IR analytical device. Catalysts containing up to about 1 $atom_{Cu}\ nm^{-2}$ displayed very little activity, while catalysts with higher copper content were active and selective. Maximum activity was associated with samples containing 1.5−2 $atom_{Cu}\ nm^{-2}$, while samples with higher copper concentration were less active. Results point to the need to individuate relationships between structure and catalyst properties and activity to optimize the preparation of suitable tailored copper-containing catalysts.

Introduction

It is recognized that the process of selective reduction of NO_x by C_1-C_4 hydrocarbons in an oxidizing atmosphere (HC-SCR) is more than a promising method to remove NO_x from lean-burn and diesel exhausts. The lean exhaust typical for diesel engines requires selective catalytic processes that allow for the preferential reduction of NO_x besides oxygen. They include, among others, HC-SCR,[1] SCR with N-containing reducing agents,[1,2] and the NO_x storage−reduction catalytic cycle.[3]

The chemical and mechanistic aspects of HC-SCR with the prospective drawbacks associated with the process of technological development have been extensively reviewed by many authors.[1,4−7] More recently, Yahiro and Iwamoto[8] have reviewed the historical development of HC-SCR starting from Cu-MFI, the most famous catalyst in the field of environmental catalysis. All the experimental evidence point to the superior activity of copper-exchanged zeolites compared to the relevant amorphous supported systems. A reason why copper is more active in zeolite structures (in particular ZSM5) than on amorphous oxides is that the zeolite disperses the active copper at the atomic level. Accordingly, more than one scientific group agrees with the fact that the HC-SCR depends on copper dispersion.[9,10] In particular, compilation of results reported by Bethke et al.[11] shows that HC-SCR is primarily affected by the nature of the copper centers and not by the nature of the support. Moreover, the study of Márquez-Alvarez et al.[12] performed on Cu−ZSM5 and $Cu-Al_2O_3$ catalysts by XANES spectroscopy with interpretation by factor analysis showed that the HC-SCR can be performed in any Cu-based system containing small cupric oxide particles and some acidity. Desirable support properties are high mechanical and hydrothermal stability.

The catalyst preparation method is a critical factor for improving the de-NO_x activity of copper dispersed catalysts together with the choice of a suitable support with acidic properties and a wide surface to disperse the copper phase. Particularly for $Cu-Al_2O_3$ systems, a large dependence on the catalyst preparation method was found. A recent report of Chen et al.[13] showed the interesting activity of the $Cu-Al_2O_3$ system and the comparison among four differently prepared $Cu-Al_2O_3$ samples (conventional impregnation, coprecipitation, evaporation of mixed aqueous solution, and xerogel methods). The xerogel prepared catalyst (with 5 wt % of Cu content) showed the highest activity; it was poorly affected by the presence of water and was tolerant to sulfate deposition. On the other hand, it has also been shown that basic solution preparations favor the formation of highly dispersed CuO-like aggregates on Al_2O_3, thus enhancing the catalytic activity.[14]

* Corresponding author. A.Gervasini, Dipartimento di Chimica Fisica ed Elettrochimica, Università degli Studi di Milano, via Camillo Golgi n. 19 − I-20133 Milano, Italy. Phone: +39 0250314254. Fax: +39 0250314300. E-mail: antonella.gervasini@unimi.it.

[†] Dipartimento di Chimica Fisica ed Elettrochimica, Università degli Studi di Milano.

[‡] CNR ISTM, c/o Dipartimento di Chimica Inorganica, Metallorganica ed Analitica, Università degli Studi di Milano.

10.1021/jp022064x CCC: $25.00
Published on Web 05/13/2003

TABLE 1: Copper Loading and Texture Characteristics of Catalysts

code	Cu loading: wt Cu (%)	Cu loading: wt CuO (%)	Cu loading: D_{Cu}[a] ($atom_{Cu}$ nm^{-2})	surface area (m^2 g^{-1})	porosity[b] (cm^3 g^{-1})
SA				484.8	0.791
Cu−SA02	0.23	0.29	0.042	514.9	0.857
Cu−SA04	0.41	0.51	0.080	487.5	0.819
Cu−SA1	1.27	1.59	0.241	499.8	0.835
Cu−SA5	4.95	6.20	1.111	422.1	0.791
Cu−SA7	7.26	9.09	1.999	344.3	0.671
Cu−SA9	8.70	10.89	2.633	313.2	0.684
Cu−SA12	12.4	15.52	3.687	318.8	0.654

[a] Copper density calculated as amount of Cu introduced per unit surface. [b] Determined from desorption branch of N_2 adsorption isotherm by BJH model.

The chemisorption−hydrolysis (Ch-Hy) method has been found to be very effective for the preparation of very well dispersed supported copper species, as shown by transmission electron microscopy (TEM), temperature-programmed reduction (TPR), and FT-IR of adsorbed CO and UV−Vis−NIR spectroscopies.[15,16] Our recent results[17] showed promising activity in the selective reduction of NO of Ch-Hy prepared copper catalysts supported on pure and modified silicas (SiO_2, SiO_2−Al_2O_3, SiO_2−TiO_2, and SiO_2−ZrO_2). The catalyst prepared on SiO_2−Al_2O_3 (1.5 wt %) had the best activity and selectivity (40% of NO_x conversion to N_2, 86% of C_2H_4 conversion to carbon oxides at 573 K and at 9 g s $mmol^{-1}$ of contact time). Interestingly, on this catalyst, turnover frequency values for the HC-SCR with ethene were close to those of other copper dispersed systems (CuO_x/ZrO_2) and of Cu−ZSM5.[9] On this basis, a deeper investigation on a series of supported copper-based catalysts prepared by the Ch-Hy method has been performed. A similar support than that previously used, namely, a SiO_2−Al_2O_3 containing 13 wt % of Al_2O_3, was employed, and the copper loading was varied in the range 0.2−12 Cu wt %. Here we report the obtained results in terms of characterization of bulk and surface catalyst properties and of de-NO_x activity, aimed at establishing structure−activity relationships, for a better knowledge of copper-based catalysts for SCR reaction.

Experimental Section

Sample Preparation. The silica−alumina support (SA) with 13 wt % Al_2O_3 content was kindly supplied from Grace Davison, Worms (D) and it was used without any thermal treatment. The copper catalysts, hereafter referred to as Cu−SAX (in the code the last figure indicates the copper loading, see Table 1), were prepared by what was called in previous papers[15−17] the chemisorption−hydrolysis (Ch-Hy) method. In the preparation, the support was added to a $[Cu(NH_3)_4]^{2+}$ solution prepared by adding NH_4OH to a $Cu(NO_3)_2 \cdot 3H_2O$ solution of suitable concentration until pH 9. After 20 min under stirring, the slurry, held in an ice bath at 273 K, was slowly diluted to allow hydrolysis of the copper complex and deposition of the finely dispersed product to occur. The solid was separated by filtration, washed with water, dried overnight at 383 K, and calcined in air at 623 K for 4 h.

Characterization Techniques and Procedures. The copper content of the samples was measured by atomic absorption spectrometry (AA) analysis after dissolution in HNO_3. The copper loading of each catalyst is reported in Table 1 expressed as wt % Cu and CuO and as density of Cu per unit surface (D_{Cu}, $atom_{Cu}$ nm^{-2}).

The nitrogen adsorption/desorption isotherms were obtained at liquid nitrogen temperature (77 K), using a Sorptomatic 1900 version instrument from Thermoquest. Prior to the determination of the adsorption isotherm, weighed portions of each sample (0.05 g) were outgassed for 16 h at 623 K under a residual pressure of 10^{-2} Torr to remove moisture. Nitrogen was 99.9995% purity. The adsorbed volume, expressed in cm^3 (STP) g^{-1}, was converted into pore volume, cm^3 g^{-1}, using the density of N_2 in the normal liquid state ($\rho = 0.8081$ g cm^{-3}). Molecular area of N_2 was taken as 16.2 $Å^2$.

Scanning electron micrographs (SEM) were obtained with a Cambridge Stereoscan 150 instrument able to give magnifications of 100 000. The tungsten wire was saturated with 3 A of intensity current and the electrons were accelerated with a ddp of 20 kV. The samples were coated with gold, and the micrographs of the particles were taken with a Polaroid camera.

XRD diffraction analyses on the powder samples in atmospheric air were collected with a Philips PW1710 vertical goniometric diffractometer using a Ni-filtered Cu $K_{\alpha 1}$ radiation ($\lambda = 1.54178$ Å). The ionization chamber rotated around the sample at 1° 2θ min^{-1}; the interval range of investigation was from 5° to 75° 2θ.

Diffuse reflectance spectroscopy (DRS) spectra were recorded at room temperature (RT) in the wavelength range 250−1300 nm (scanning rate of 100 nm·min^{-1}), covering UV and visible region (1 eV = 96.48 kJ mol^{-1} = 8065 cm^{-1}), using a JASCO V-570 spectrometer with $BaSO_4$ as reference equipped with microcomputer for data acquisition and analysis.

X-ray photoelectron spectra (XPS) were collected in an M-Probe apparatus (Surface Science Instruments). The X-ray source provided monochromatic Al K_α radiation (1486.60 eV). The residual pressure in the analysis chamber was typically 5 $\times$ 10^{-9} Torr. Charge effects were compensated by the use of a flood gun (3 eV). A spot size of 400 $\times$ 1000 μm and a pass energy of 150 eV were used for survey spectra, while for the single-region acquisitions a spot size of 200 $\times$ 750 μm and a pass energy of 25 eV with 0.74 eV resolution were used. The Si 2p line from silica (103.3 eV) was used as internal reference with an accuracy of $\pm$ 0.20 eV. The quantitative analysis was performed using the sensitivity factors given by Scofield[18] from the intensities of Cu $2p_{3/2}$, Si 2s, and Al 2p. The XPS peaks were decomposed using a peak-fitting routine. The lines used in the fitting of a peak envelope are defined according to their centered position, half-width, shape (Gaussian or Lorentzian distribution), and intensity. The best fit of the experimental curve by a tentative combination of bands was searched.

Redox cycles (TPR1/TPO/TPR2) were realized carrying out in sequence, a first temperature programmed reduction (TPR) on the oxidized sample (TPR1), a temperature programmed oxidation (TPO), and a second temperature programmed reduction (TPR2). A TPDRO-1100 (CE instruments) equipped with a quartz reactor with a porous septum (ca. 8 mm i.d.) and a filter filled with soda lime for trapping acid gases and water were employed.[19] Prior to the TPR1 run, the fresh sample was treated in a stream of O_2/N_2 (20% v/v, flowing at 45 cm^3 min^{-1}) ramping the temperature at 8 K min^{-1} from RT to 623 K and maintained it for 60 min, and then cooling at 313 K. TPR1 measurement was carried out using H_2/Ar (4.98% v/v) as reducing gas mixture, flowing at 14 cm^3 min^{-1} with a thermal conductivity detector (TCD) for measuring the amount of H_2 uptake. Heating rate was 8 K min^{-1} from 313 to 800 K or to 1000 K. The TPO run was carried out on the reduced sample (after TPR1) cooled at 313 K in H_2/Ar flow. After a purge with Ar (10 cm^3 min^{-1}), the oxidizing gas mixture composed of O_2/He (5.02% v/v) flowed at 14 cm^3 min^{-1} through the sample from 313 to 800 K. The oxidized sample was further reduced

by the TPR2 run, under the same experimental conditions described above.

Sample size used was adjusted to have around 40 μmol of CuO independently of the Cu loading of samples. This allowed us to maintain K and P values[20,21] around 100 s and 10 K, respectively, for all the analyses, except for Cu−SA02 and Cu−SA04, for which values of K and P around 25 s and 3 K, respectively, were used due to the very poor Cu content.

TPR peak areas were calibrated employing CuO bulk standard per analysis as reference material or pure H_2 (Sapio, Italy; purity >99.9999%) injections. The amount of H_2 consumed gave the reduction extent, $(H_2/Cu)_{mol}$. The average oxidation number (n_{av}) of Cu was calculated as $n_{av} = 2 - 2(H_2/Cu)_{mol}$.

Catalytic Activity. The catalytic tests were carried out with samples of mass around 0.30 g sieved as particles of 0.25−0.35 nm and introduced in a quartz tubular microreactor (5 mm ID). The reactant stream was provided from a set of mass flow controllers (Bronkhorst, Hi-Tec) supplying 1500 ppm of NO and of C_2H_4, and 15 000 ppm of O_2 in helium at a total flow rate of 50 cm^3(STP) min^{-1}, with the reactor at close to atmospheric pressure. The contemporary presence in the feed mixture of NO with high O_2 amount gave rise to an effective feed composition constituted of both NO and NO_2, i.e., NO_x mixture. Typical real concentrations were around 1350 ppm of NO, 150 ppm of NO_2, 1500 ppm of C_2H_4, and 15 000 ppm of O_2. Contact time was maintained constant at 8 g s $mmol^{-1}$. Eight plateaus in the interval of reaction temperature from 473 up to 723 K were investigated; every run lasted about 18 h. The samples were contained in the reactor between plugs of quartz wool and initially pretreated in flowing 20% v/v of O_2/He while raising the temperature in stages up to 623 K and maintaining it for 4 h.

The exit gas stream from the reactor flowed through a gas cell (path length 2.4 m multiple reflection gas cell and 100 cm^3 of volume) working at room temperature in the beam of an FTIR spectrometer (Bio-Rad with DTGS detector). In typical experiments, the residence time in the gas cell was around 120 s. The spectrometer permitted the analyses of NO, N_2O, and NO_2 for N-containing species, and of C_2H_4, CO, and CO_2 for C-containing species. The measurements were carried out at 0.50 cm^{-1} resolution, with an accumulation of 19 scans per spectrum. The gas cell gave an accuracy of ± 10 ppm for NO, and ± 4 ppm for N_2O and for NO_2 using lines at 1876, 2225, and 1619 cm^{-1}, respectively. The operative methodology provided the monitoring of the absorbance of all the IR active species (Gram-Schmidt) flowing from the reactor each 120 s. The absorbance profile of each species detected as a function of time/temperature of reaction was determined on the basis of the chosen wavelength of absorption of the species from the decomposition of the Gram-Schmidt plot. The use of the FT-IR spectrophotometry for monitoring the species concentration flowing inlet and outlet from the reactor during an SCR reaction has been already reported in the literature.[22] For each IR-active species, good linearity of the absorbance as a function of the concentration into the gas cell was observed. The slopes of the lines obtained, relating to the molar extinction coefficients, permitted the quantification of the outlet concentrations from the reactor. Blank tests with the empty reactor showed the conversion of NO to NO_2 by homogeneous oxidation with our used standard mixture (about 10%).

SCR activity in terms of N_2 formation was determined subtracting the sum of all the N-containing species flowed out from the reactor from the sum of all the N-containing species fed into the reactor. On the basis of N_2 concentration (ppm), the specific integral rate (r_{N2}) was calculated and expressed as $mmol_{N2}\ g_{cat}^{-1}\ s^{-1}$. Selectivity to the N_2 was evaluated as the ratio between the amount of C_2H_4 consumed to reduce NO_x to N_2 and the total amount of C_2H_4 consumed, thus obtaining the so-called competitiveness factor (S_{SCR}, %).[11,23] Concerning the C-containing species, satisfactory carbon balances were calculated for low reaction temperatures for all the catalysts, while at the highest temperatures non-negligible carbon loss together with opalescence of the FTIR gas cell were observed. This can be imputable to oxime formation that has been recognized as an intermediate of SCR of NO_x by Beutel et al.[24] Recently, Wu and Larsen[25] have corroborated this evidence by a solid-state nuclear magnetic resonance study.

TABLE 2: Surface Copper Presence as Determined by XPS Analysis

	BE (eV)	atom concentration[a] (%)			
code	Cu $2p_{3/2}$	Cu_{2p}	Al_{2p}	Si_{2s}	$[Cu_{2p}/(Si_{2s} + Al_{2p})]$ (%)
SA		n.d.	16.7	83.3	0
Cu−SA02		n.d.	16.6	83.4	0
Cu−SA04		n.d.	16.0	84.0	0
Cu−SA1		n.d.	18.4	81.6	0
Cu−SA5	933.91	2.6	30.1	67.3	2.67
Cu−SA7	933.27	3.7	20.5	75.8	3.84
Cu−SA9	933.15	3.3	31.0	65.7	3.41
Cu−SA12	933.74 936.14	5.4	36.6	58.0	5.71

[a] Normalized values ruling out the O and C atoms determined.

Results and Discussion

Catalyst Preparation and Aspect. Highly acidic silica−alumina (SA) used as support for the copper deposition had about 3 meq of acid sites per unit mass, of which 67% can be considered as weak sites (temperature of desorption around 450 K) and 33% as strong acid sites (temperature of desorption around 750 K), as determined from 2-ethyl phenylamine desorption by thermogravimetric experiments.[26] The acidic strength of SA can be considered as a bimodal type. The evidence of Al presence at the surface (from XPS analysis, see Table 2) could support the hypothesis of Brœnsted, for weak, and Lewis, for strong, acid sites presence on SA surface.

The copper loading on SA support was simply tuned by varying the $Cu(NO_3)_2$ initial solution concentration but keeping the pH of the $Cu(NH_3)_4^{2+}$ at a constant value of 9. The amount of Cu deposited on silica−alumina support was determined by AA analysis, and the results are presented in Table 1 in terms of Cu and CuO wt %. A very large range of Cu loading varying from 0.23 to 12.4 wt % is present. The increasing Cu concentration is related to color variation of the calcined catalysts. The catalysts containing the lowest Cu amount (Cu−SA02 and Cu−SA04) are pale blue, while the color turns bright light blue for CuSA-1 and Cu−SA5, blue-green for the Cu−SA7 and Cu−SA9, and green for the highest Cu containing catalyst (Cu−SA12). This behavior could be indicative of the existence of Cu^{2+} species, for low copper concentration, and $[Cu-O-Cu]^{2+}$ oxocations for higher values. Beutel et al.[27] have demonstrated by several techniques that high Cu loading is a condition for the existence of oxocation structures; samples in which these structures have been identified are green, while low Cu content is consistent with the Cu^{2+} presence and blue color.

The external morphology of the low concentrated Cu catalysts, as it appeared in the electron micrographs (SEM), is typical of highly dispersed CuO_x aggregates sparsely covering the SA support. Quite the same aspect can be observed for the more concentrated Cu catalysts that maintained a high dispersion of

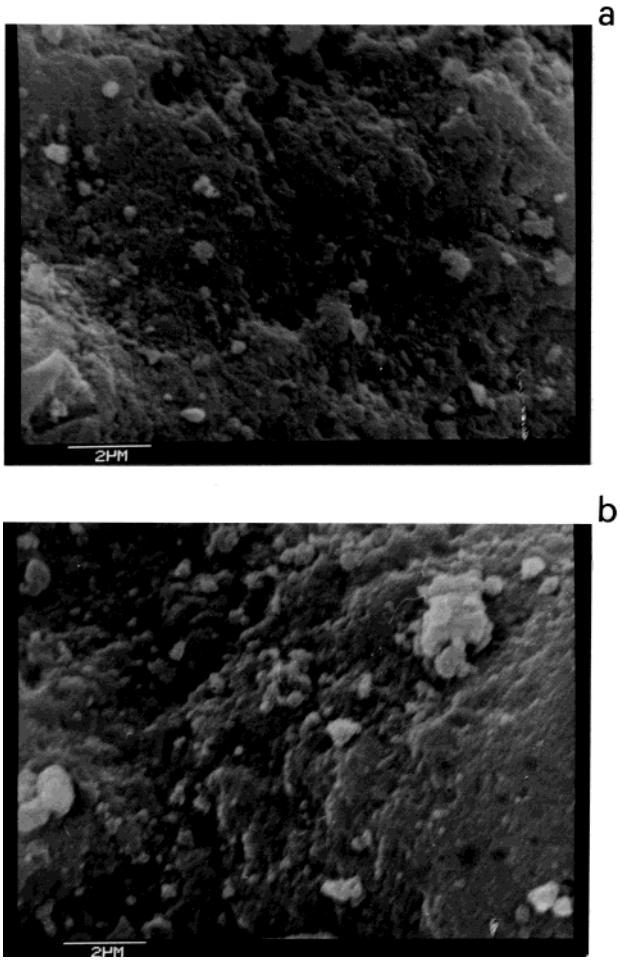

Figure 1. Scanning electron micrographs of Cu−SA5 (a) and Cu−SA12 (b) catalysts at 10 000 magnifications.

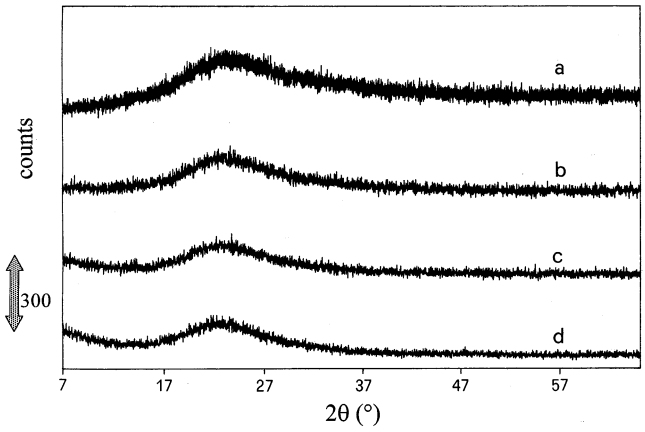

Figure 2. XRD patterns of the catalysts containing copper at different concentration. Cu−SA12 (a), Cu−SA7 (b), Cu−SA5 (c), Cu−SA1 (d).

the Cu phase, as shown from the micrographs of Cu−SA5 and Cu−SA12 (Figure 1). No significant differences could be observed between the micrographs of Cu−SA5(7,9,12) in terms of CuO_x size, even if the CuO loading of Cu−SA12 is more than 2-fold that of Cu−SA5. Results from XRD analyses are in agreement with the evidence obtained from SEM images. Both the low and the high concentrated CuO_x containing catalysts presented XRD patterns typical of amorphous solids without any XRD lines related to separate CuO phase or metal oxide clusters (Figure 2). This did not exclude the presence of very small oxide clusters of several nanometers in size that do not show X-ray diffraction.

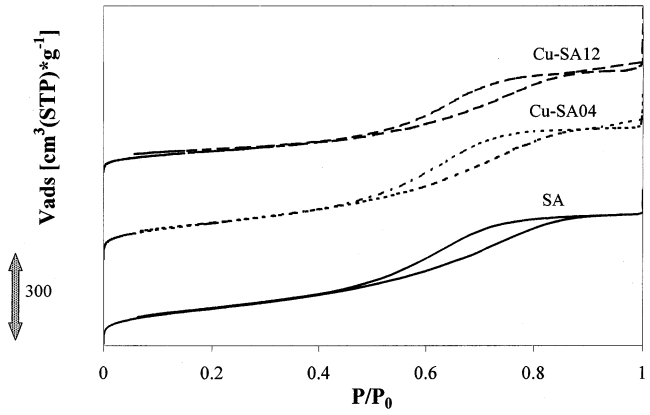

Figure 3. Adsorption/desorption isotherms of N_2 at 77 K over the silica−alumina (SA) support and over two catalysts at low (Cu−SA04) and high (Cu−SA12) copper concentration.

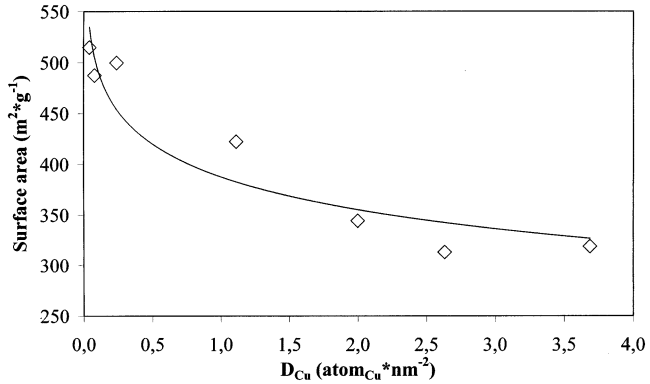

Figure 4. Surface area (BET) values for the series of copper catalysts on silica−alumina support as a function of Cu density (D_{Cu}, expressed as $atom_{Cu}$ nm^{-2}).

Characterization of the Samples. *Textures of Samples.* The silica−alumina used as support belongs to type IV (mesoporous solid in which capillary condensation takes place at higher pressures of adsorbate in addition to multiplayer adsorption at lower pressures), according to IUPAC classification.[28] Mean porous wideness of the oxide is centered around 33 Å of pore radius (Figure 3 and Table 1). Deposition of CuO on SA did not deeply modify the shape of the N_2 isotherms of the support. Concerning the values of pore volumes and average pore radii, differences among the catalysts could be observed. By increasing the Cu content on the support, lowering of both pore volumes and surfaces was detected indicating the increasing covering of SA by CuO_x aggregates located on free surface and on interparticle voids of the support. Comparing the results for Cu−SA02 and Cu−SA12, a decrease of 24 and 38% of porosity and surface area, respectively, was observed for Cu−SA12 compared to Cu−SA02. In light of the very large differences of CuO loading between the two samples (0.3 and 15.5 Cu wt % for Cu−SA02 and Cu−SA12, respectively), the contraction does not appear notable. Once the amount of copper loading and the catalyst surface are known, it is possible to calculate the copper density (D_{Cu} in $atom_{Cu}$ nm^{-2}). D_{Cu} values are most effective for representing the Cu surface loading, and they will be used in the following in relation to the physical and chemical properties of the samples. Figure 4 presents the exponential trend of the catalyst surface area values as a function of copper density for all the samples. The decreasing exponential trend is indicative of a good copper dispersion. In fact, the deposition of the amount of CuO up to about 5−6 wt % caused a marked decrease of the catalyst surface, probably due to CuO_x species

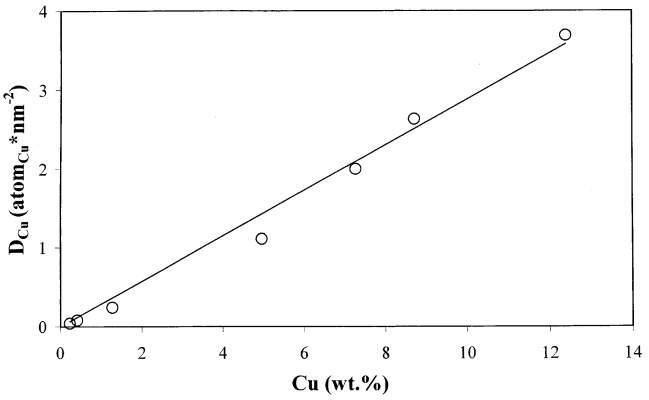

Figure 5. Copper density (D_{Cu}, expressed as atom$_{Cu}$ nm^{-2}) as a function of Cu loading (wt %) for the series of catalysts studied.

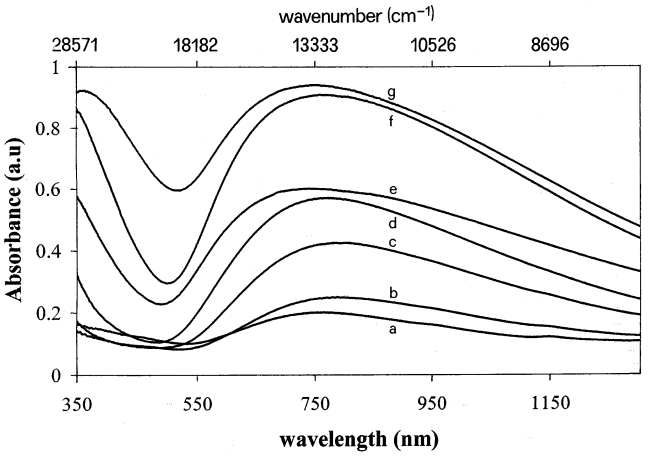

Figure 6. DRS spectra of the copper containing catalysts. Cu−SA02 (a), Cu−SA04 (b), Cu−SA1 (c), Cu−SA5 (d), Cu−SA7 (e), Cu−SA9 (f), and Cu−SA12 (g).

location in the support interparticle voids, as discussed above. For higher CuO deposition (up to 15 wt %), the decrease of surface area of the catalysts was lighter due to the formation of ever smaller CuO_x aggregates, of nanosized diameter, on free surface of the support. SEM images, discussed above, are in agreement with this picture. Figure 5 confirms the spreading of CuO_x aggregates on the SA surface irrespective of the Cu loading by the good linear trend of D_{Cu} as a function of the Cu loading. Deviation from linearity would have been observed if the increasing Cu content caused abrupt variation of catalyst texture.

DRS Characterization. The UV−vis spectra recorded in diffuse reflectance (DRS) of the calcined copper containing catalysts consisted of an asymmetric band at 600−1000 nm due to d−d transitions of dispersed Cu^{2+} species (3 d^9).[29,30] The d−d bands are of low intensity for the lowest Cu concentrated catalysts and their intensity increased with Cu content (Figure 6). The observed d−d transitions were in the range expected for Cu^{2+} species in an axially distorted octahedral environment of O-containing ligands.[31] The values of maximum wavelength (λ_{max}) for the d−d transitions were decreasing from 818 nm for Cu−SA02 to 807, 789, 771, 767, 759, and 754 nm for Cu−SA04, Cu−SA1, Cu−SA5, Cu−SA7, Cu−SA9, and Cu−SA12, respectively. The shift at lower wavelengths of the absorptions with increasing copper concentration suggests an increasing nuclearity of the oxidic clusters (CuO_x species). It should be noted that the presence of small but defined CuO particles would have given d−d transitions shifted to lower wavelengths losing the asymmetric character.[29] No evidence of absorption edges

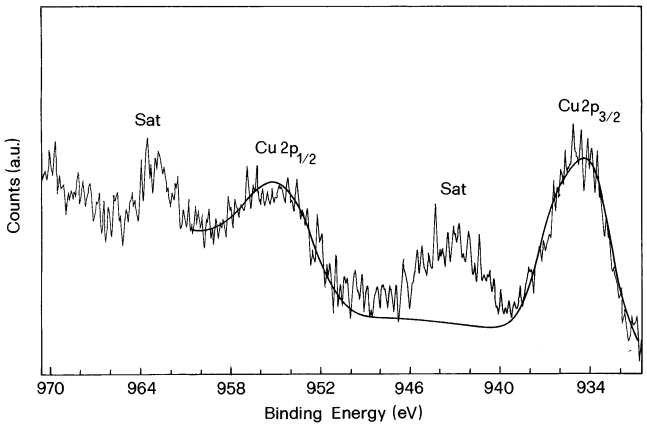

Figure 7. Cu 2p XPS spectrum of the Cu−SA12 sample.

at ∼650 nm or at ∼890 nm, due to the energy gap of large particles of Cu_2O ($E_g \approx 15\,320$ cm^{-1}) and of CuO ($E_g \approx 11\,290$ cm^{-1}), respectively, was present in the spectra. At lower wavelength, the DRS are dominated by strong absorption in the 300−500 nm interval, with maxima clearly distinguished for Cu−SA7 (330 nm), Cu−SA9 (346 nm), and Cu−SA12 (363 nm) due to O^{2-} to Cu^{2+} charge-transfer transitions.

The DRS spectral evidence is consistent with the hypothesis that on the studied catalysts most of the copper is in the form of dispersed 6-coordinated Cu^{2+} species.[32,33] CuO_x-like species at low nuclearity could be present in dispersed form even at high Cu loading (more than 8 wt % of CuO). Analogous bands have been detected on dilute (around 3 atom$_{Cu}$ nm^{-2}) CuO_x/ZrO_2[27] and CuO_x/Al_2O_3[34,35] systems; accordingly, they have been assigned to Cu(II) species in axially distorted octahedral sites.

XPS Characterization. The binding energy of Cu $2p_{3/2}$ of the CuO-based catalysts are listed in Table 2, and the values agree with those reported for various Cu^{2+} containing systems dispersed on oxide phases.[36,37] XPS analyses were repeated on more than one portion of each sample, and all the results confirm that Cu was not detectable at the surface up to its density of about 1 atom$_{Cu}$ nm^{-2}. The main XPS features of the Cu catalysts are the appearance of spin−orbit split Cu $2p_{1/2}$ and Cu $2p_{3/2}$ peaks along with their shake-up satellites as characteristic for Cu^{2+}.[36−38] The intensity ratio of the satellite peak to the corresponding principal peak (I_{sat}/I_{pp}) was found to be about 0.5 only for the most concentrated copper sample (Cu−SA12). Conversely, the I_{sat}/I_{pp} ratio was markedly lower for all the other catalysts at lower copper concentration. Low I_{sat}/I_{pp} values suggest that the highly dispersed CuO_x species should be located in an octahedral coordination environment, while for Cu−SA12, the CuO_x species change their coordination environment.[35] Moreover, the Cu−SA12 sample (Figure 7) presents two contributions to the Cu $2p_{3/2}$ peak: one at 933.74 eV and the other at 936.14 eV. The shift at high binding energy is indicative of a charge transfer from the metal ion toward the support oxide.[39] In agreement with similar observations reported by Córdoba et al.[37] on CuO−TiO_2 samples, the two signals can be associated with CuO (933.74 eV) and Cu−O−Si−O− (936.14 eV) species. Relatively strongly acidic groups (−Si−OH−Al−) or weakly acidic ones (−Si−OH) together with Lewis sites related with defective aluminum sites could be present on the surface of silica−alumina. Depending on the Cu loading, different Cu−support interactions occurred leading to Cu-phase dispersed in a different way and possessing different acidity.

From the atomic concentrations reported in Table 2, it is possible to calculate the surface Al/Si ratio $(Al/Si)_s$ and compare

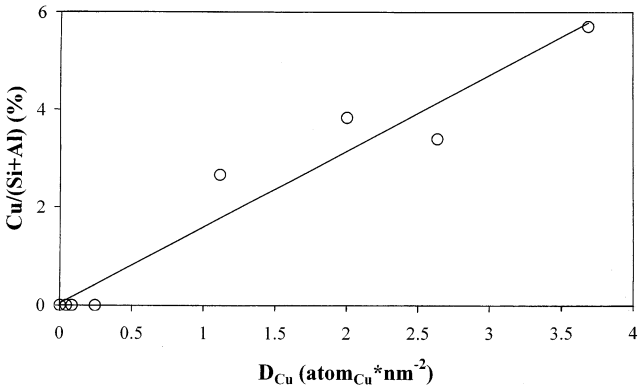

Figure 8. XPS quantitative analysis result as a function of copper density (D_{Cu}, expressed as $atom_{Cu}$ nm^{-2}).

TABLE 3: Reduction Results of CuO-Based Catalysts from TPR1 Analysis

code	T_m of TPR peak (K) [a]			reduction extent $(H_2/Cu)_{mol}$ [b]
	$T_{m,1}$	$T_{m,2}$	$T_{m,3}$	
Cu−SA02	n.d.	n.d.	n.d.	n.d.
Cu−SA04		650.3 (26.6)	896.3 (73.4)	1.0.
Cu−SA1		640.5 (39.7)	845.7 (60.3)	1.0.
Cu−SA5	571.9 (24.6)	664.4 (75.4)		1.0
Cu−SA7	530.8 (33.4)	604.8 (66.6)		0.8
Cu−SA9	539.0 (37.6)	568.7 (62.4)		0.9(5)
Cu−SA12	516.9 (100)			0.8
CuO−SA[c]			714.0 (100)	0.3

[a] Percent peak area is indicated into brackets. [b] mol of H_2 consumed per Cu mol. [c] Physical mixture of CuO and SA.

it with the relevant bulk Al/Si ratio $(Al/Si)_b$. For the SA support and the catalysts at low-medium copper density (up to ca. 2 $atom_{Cu}$ nm^{-2}) the values of $(Al/Si)_s$ and $(Al/Si)_b$ are in accord, while for the samples at higher copper density the $(Al/Si)_s$ values increase suggesting a preferred covering of the CuO_x species on -SiO_2- portions of the $SiO_2-Al_2O_3$ surface. At a first approximation, it seems that the presence of -Al_2O_3- on the surface does not act as preferential attack point for the copper phase.

When the $Cu_{2p}/(Si_{2s}+Al_{2p})$ intensity ratios, experimentally determined from the peak areas of the elements corrected by the relevant Scofield sensitivity factors, are reported as a function of Cu content up to more than 3 $atom_{Cu}$ nm^{-2} (Figure 8), a linear trend could be individuated. This behavior suggests that the copper species were uniformly spread on $SiO_2-Al_2O_3$ surface. Segregation of copper would have caused lower experimental $Cu_{2p}/(Si_{2s}+Al_{2p})$ values with deviation from linearity.

Redox Cycles with Temperature Programmed Reduction and Oxidation. The reversibility in a redox cycle of the CuO_x centers of the studied catalyst series was investigated by TPR and oxidation analyses (TPR1/TPO/TPR2 cycle). Table 3 summarizes the most significant results, in terms of maximum temperatures (T_m) of the reduction peaks and of the CuO reduction extent, $(H_2/Cu)_{mol}$, calculated on the basis of hydrogen consumption, for the TPR1 analyses. The reduction profiles obtained for Cu−SA02 were of so low intensity that it was not possible to univocally assign any temperature and hydrogen uptake. Starting from Cu−SA04, the assignments could be made with accuracy.

Two reduction peaks at very high temperatures with T_m values at ca. 645 K and at ca. 860 K (indicated in Table 3 as $T_{m,2}$ and $T_{m,3}$, respectively) were observed for Cu−SA04 and Cu−SA1 (D_{Cu} in the 0.08−0.24 $atom_{Cu}$ nm^{-2} range). The $T_{m,3}$ peak is anomalously high even if compared with the reduction peak of bulk CuO (Table 3). It is known that,[40] when the reduction of very low Cu concentration samples is concerned, sublimation phenomena of copper species can perturb the reduction process. At the beginning of reduction, very small particles of metallic copper are formed because the sintering is hampered by a good dispersion and isolation of the CuO_x species. As the TPR run proceeds, the small particles of metallic copper could have enough energy to sublime, thus covering the unreduced CuO_x species. The reduction of the CuO_x phase is probably hindered by the metallic copper film, the hydrogen having to diffuse through it before reducing CuO_x, thus leading to increase of the observed reduction temperatures. When the Cu loading is high enough, sublimation can be avoided. In fact, the peak with $T_{m,3}$ was 73% for Cu−SA04 and decreased to 60% for Cu−SA1, and then it was no more observed for the more concentrated catalysts. On the opposite hand, the peak with $T_{m,2}$ is more intense for Cu−SA1 than for Cu−SA04. The position of the $T_{m,2}$ peaks is compatible with the presence of small and well-dispersed CuO_x species. Starting from Cu−SA5 (1.111 $atom_{Cu}$ nm^{-2}), besides $T_{m,2}$ reduction peak, a lower temperature peak appeared ($T_{m,1}$). The most concentrated Cu catalyst (Cu−SA12) displayed one well-resolved peak at low temperature ($T_{m,1}$). The proportions between $T_{m,1}$ and $T_{m,2}$ peaks are reported in Table 3. The areas of $T_{m,1}$ peak increased from 25% for Cu−SA5 up to 100% for Cu−SA12. On the opposite hand, the areas of $T_{m,2}$ peak decreased from 75% for Cu−SA5 down to 62% for Cu−SA9, and then the peak vanished for Cu−SA12. Referring to the literature,[27,41] it seems reasonable to suggest that the low-temperature peak ($T_{m,1}$) corresponds to more easily reduced Cu species than those associated with the $T_{m,2}$ peak; the structure of the species associated with $T_{m,1}$ could be of oxocations-like type, $[Cu-O-Cu]^{2+}$. When one considers the $T_{m,1}$ and $T_{m,2}$ peak area percents as a function of D_{Cu} values, increasing and decreasing (starting from Cu−SA5) trends could be observed, respectively, pointing to an intersection point consistent with the maximum dispersion capacity of the SA support around 2.5 $atom_{Cu}$ nm^{-2}. When the loading of CuO exceeds the SA dispersion capacity, existence of Cu centers in closer interaction occurs.

Percent of reduction, calculated from the sum of the two reduction peaks ($T_{m,2}$ and $T_{m,3}$ or $T_{m,1}$ and $T_{m,2}$), was very close to 100% for the low Cu-containing catalysts and then it became less satisfactory by increasing the Cu content (Table 3). In every case, the average oxidation number of the reduced Cu centers was close to zero. As a general trend, the CuO_x species deposited on SA constitute an easily reducible phase, independently of the nature and extension of the aggregates formed.

Oxidation by TPO of the reduced samples showed profiles that did not differ among them in a remarkable way. In every case, two TPO peaks were observed in the 400−550 K interval, confirming the presence of Cu species with a different nature deposited over the support. A second reduction analysis (TPR2) was performed on the oxidized samples. Figure 9 comparatively presents the collected reduction profiles. In the figure, the results for Cu−SA02 and Cu−SA04 have been ruled out due to the poor quality and the very low intensity of the collected curves, as mentioned above. The shape and position of the TPR2 profiles are markedly different among catalysts. Moreover, pronounced differences emerged between the TPR1 and TPR2 profiles, that are very more marked for the low Cu concentrated samples. TPR2 profiles appear at lower temperatures than TPR1 ones, and the distance in temperature between the two profiles decreased as the Cu content increased. The highest Cu contained catalyst showed quite the same profiles for the first and the second reductions in terms of peak shape and position. The lack of overlapping between TPR1 and TPR2 analyses suggests a

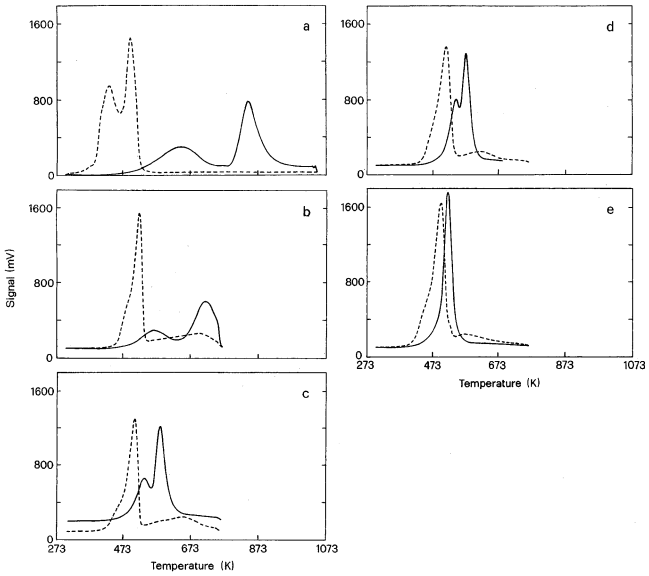

Figure 9. TPR profiles of the reduction of CuO_x in catalysts at increasing CuO loading. Experiments were made using a catalyst mass corresponding to definite amount of CuO: 44.47 μmol for Cu−SA1 (a), 35.73 μmol for Cu−SA5 (b), 31.77 μmol for Cu−SA7 (c), 38.32 μmol for Cu−SA9 (d), and 46.29 μmol for Cu−SA12 (e). TPR1 (solid lines) and TPR2 (dotted lines).

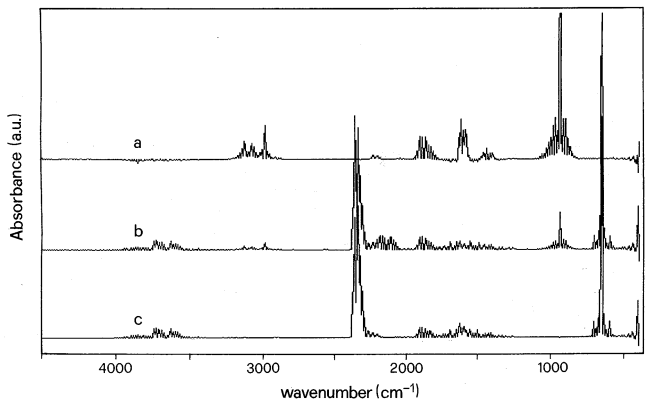

Figure 10. FTIR spectra of streams from the reactor over Cu−SA5: feed (a), downstream at temperature of maximum NO_x conversion (b), and downstream at maximum reaction temperature (c).

mobility of the CuO_x species leading to more aggregated CuO_x centers. The reducibility of these new created Cu species was high, as confirmed by the low reduction temperatures. Mobility of CuO_x species diminished by increasing the Cu content, as larger CuO_x aggregates were present on fresh samples.

Catalytic Study of NO_x Reduction. The series of catalysts at different Cu loading has been studied in the SCR of NO_x with C_2H_4 as reducing species in lean conditions in the 473−723 K temperature range at fixed contact time (8 g s mmol^{-1}). Figure 10 (spectrum a) shows a chosen example of FTIR spectrum for a typical feed composition in which the absorbance peaks of the N-containing species are well evident. The spectrum is dominated by the intense peak of NO (1875.99 cm^{-1}), and a less intense one is due to NO_2 (1618.64 cm^{-1}). N_2O (2224.85 cm^{-1}) was always present in the feed as well as in all the successive spectra of the outstreams from the reactor independently of the type of catalyst, and it did not follow a clear increasing or decreasing trend with reaction temperature. Spectra b and c of Figure 10 show the outstreams at temperature of maximum NO_x conversion and at the highest reaction temperature, respectively, for Cu−SA7 catalyst, chosen as an example

TABLE 4: Exit Gas Composition and Main Results from the Reaction of 1500 ppm of NO_x (ca. 1350 and 150 ppm of NO and NO_2), 1500 ppm of C_2H_4 and 15000 ppm of O_2 at Different Temperatures over the CuO_x-Based Catalysts

		concentration (ppm)				
code	temp[a] (K)	NO	NO_2	C_2H_4	S_{SCR} (%)	$10^5 r_{N2}$ (mmol$_{N2}$ g$_{cat}^{-1}$ s^{-1})
Cu−SA04	523	1321	90	1513	n.d.	2.26
	723	1233	76	1292	20.7	3.22
Cu−SA1	523	1383	102	1507	n.d.	2.37
	723	1159	64	1116	17.0	4.99
Cu−SA5	523	1300	0	1417	92.7	3.31
	$T_{N2,max} = 648$	891	0	494	9.9	7.44
	723	1130	0	0	4.7	5.35
Cu−SA7	523	1261	84	1364	45.5	4.91
	$T_{N2,max} = 623$	894	38	341	9.4	8.67
	723	1105	106	0	5.4	6.44
Cu−SA9	523	1219	85	1258	18.0	3.28
	$T_{N2,max} = 623$	927	47	89	5.8	6.58
	723	1076	168	0	3.3	4.05
Cu−SA12	523	1343	96	1281	15.7	2.33
	$T_{N2,max} = 648$	1119	59	30	4.7	5.08
	723	1196	179	0	2.8	3.08

[a] Temperature of maximum conversion of NO_x to N_2 ($T_{N2,max}$) is indicated, if present.

due to its high activity. The lowering of the bands at 1875.99 and 1618.64 cm^{-1} due to NO and NO_2 conversion, respectively, is well evident. The successive re-increasing of the bands at the highest reaction temperatures is due to the capture of ethene by oxygen, which prevents the further reduction of NO_x. The ethene band (951.37 cm^{-1}) continuously decreases with temperature and then vanishes, and contemporarily the band at 720.65 cm^{-1} due to CO_2 is continuously increasing.

In Table 4 significant experimental data at three different temperatures have been reported for each catalyst, except for Cu−SA02 due to its poor activity. It can be observed that starting from a given Cu loading (5 wt % corresponding to ca. 1 atom$_{Cu}$ nm^{-2}), the NO and NO_2 exit concentrations ran parallel passing through a minimum concentration, corresponding to the formation of a maximum N_2 concentration ($T_{N2,max}$). Due to this behavior, the N_2 profiles as a function of temperature were volcano-shaped curves, as known for various Cu-catalysts supported on different oxides.[9,13,17] For higher temperatures than $T_{N2,max}$, ethene was no longer present and the NO and NO_2 concentrations were increasing. On the opposite, catalysts containing very low amount of Cu (less or equal to 1 wt % corresponding up to 0.2 atom$_{Cu}$ nm^{-1}) displayed a continuously decreasing trend for the NO, NO_2, and C_2H_4 concentrations without the attainment of a definite minimum. The very poor activity of these catalysts is evidenced by the noncomplete ethene conversion even at the highest reaction temperature.

The overall trend of the SCR activity of the catalysts is depicted in Figure 11 that shows the NO_x conversion to N_2 (Figure 11A) and the C_2H_4 conversion to CO_x (Figure 11B) as a function of reaction temperature. The volcano-shaped curves of N_2 yield vs temperature are well evident for the samples with a CuO loading greater than 6%. Cu−SA5 and Cu−SA7 can be considered the most active catalysts (N_2 formation around 37%) in the SCR among the studied series. Only the most Cu concentrated catalysts (Cu−SA12, Cu−SA9, and Cu−SA7) gave total ethene consumption, because their reactivity with both NO_x and O_2. C_2H_4 is, in fact, the common reactant in the SCR reaction which can be oxidized by NO_x to give N_2[17,42,43] ($C_2H_4-NO_x$) or by O_2 ($C_2H_4-O_2$) to give rise to carbon oxides.

The N_2 selectivity, calculated according with the percent competitiveness factor (S_{SCR},%), was very high at low temperatures but it deeply decreased for high temperatures (Table 4 and

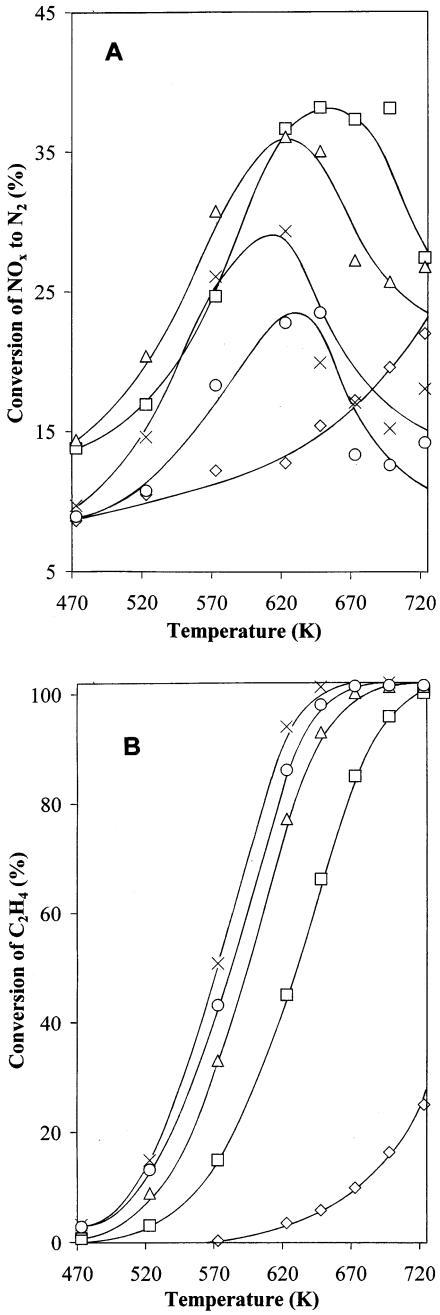

Figure 11. Conversion of NO_x to N_2 (A) and conversion of C_2H_4 to carbon oxides (B) as a function of reaction temperature in SCR (initial concentrations: ca. 1500 ppm of NO_x and of C_2H_4 and 15 000 ppm of O_2) realized at 8 g s $mmol^{-1}$ over the Cu-based catalysts: Cu−SA1 (◊); Cu−SA5 (□); Cu−SA7 (△); Cu−SA9 (X); Cu−SA12 (○).

Figure 12), irrespective of Cu concentration in the catalyst. This behavior is due to the fact that as the temperature increases, the combustion of ethene by O_2 becomes the dominant reaction in comparison with the ethene oxidation by NO_x. In fact, the SCR can be viewed as a process in which two oxidants, NO_x and O_2, compete for a limited available amount of hydrocarbon reductant.

Selectivity to CO_2 rather than to CO increased with temperature, in agreement with the enhanced combustion activity of the catalysts at high temperatures, attaining around 98−100% at the highest reaction temperatures. As a general trend, the highest selectivity to CO was observed over the low concentrated copper catalysts (up to 0.2 $atom_{Cu}$ nm^{-2}). Poor oxidation activity toward hydrocarbons besides low SCR activity characterize these low Cu containing catalysts. For the active SCR catalysts (from 1 to 3.7 $atom_{Cu}$ nm^{-2}), CO concentrations fell down to zero at temperatures around 623 K; at lower temperatures selectivity to CO was around 30−40%.

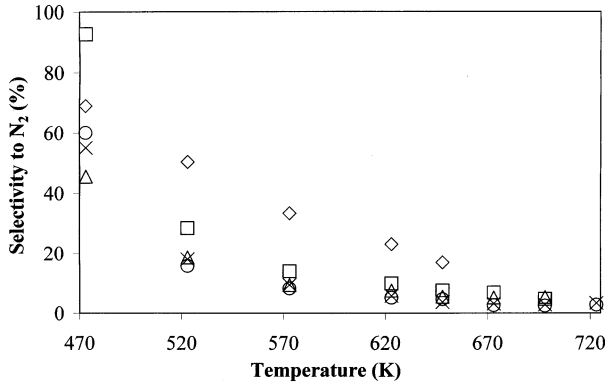

Figure 12. Trend of the selectivity to N_2, calculated according with the competitiveness factor (S_{SCR},%), as a function of reaction temperature: Cu−SA1 (◊); Cu−SA5 (□); Cu−SA7 (△); Cu−SA9 (X); Cu−SA12 (○).

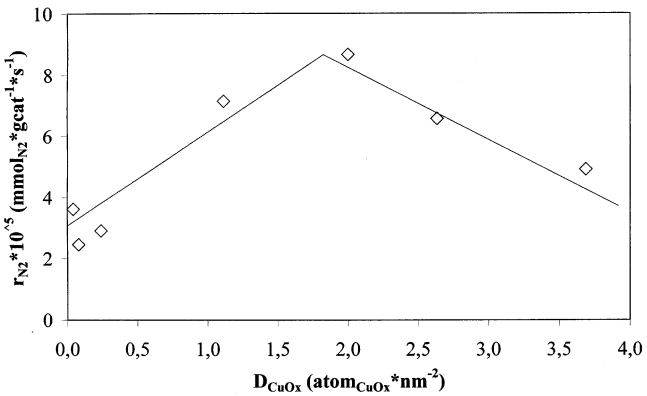

Figure 13. Trend of the specific rates of N_2 formation, r_{N2}, as a function of Cu density (D_{Cu}, expressed as $atom_{Cu}$ nm^{-2}), for all the catalysts. Each marker corresponds to r_{N2} value at 623 K

On the basis of the experimental data obtained, specific reaction rates could be calculated and expressed per mass of catalyst (r_{N2}, in $mmol_{N2}$ g_{cat}^{-1} s^{-1}) or per Cu mol (turnover frequencies, N, in $mmol_{N2}$ mol_{Cu}^{-1} s^{-1}). Confining the calculation to differential conditions (NO_x conversion not higher than 20%), differential rates could be obtained. Table 4 reports the r_{N2} values for all the catalysts at three different temperatures. The r_{N2} values at 523 K can be associated with differential rates. Cu−SA7 has two times higher r_{N2} values than Cu−SA04 (4.91×10^{-5} and 2.26×10^{-5} $mmol_{N2}$ g_{cat} s^{-1}, respectively). In fact, r_{N2} values show that the most active catalyst in terms of NO_x reduction activity to N_2 is Cu−SA7. It is interesting to view the trend of catalyst activity as a function of the Cu loading as depicted in Figure 13. The figure has been drawn reporting the r_{N2} values, calculated at 623 K, as a function of Cu content expressed in terms of Cu density (D_{Cu}). The obtained curve passes through a maximum for D_{Cu} values around 1.5−2 $atom_{Cu}$ nm^{-2}. This suggests that there is a defined suitable amount of Cu for obtaining good SCR activity, a further increase of the Cu loading favors the hydrocarbon oxidation by O_2 rather than the NO_x reduction by the hydrocarbon. This observation can be better clarified viewing the experimental results in terms of turnover frequencies (N values). It is worth noticing that the increasing of Cu by a factor of ca. 5 (Cu−SA1 and Cu−SA5 with 0.24 and 1.11 $atom_{Cu}$ nm^{-2}, respectively) leads to *N* values decreasing by a factor of about 3. Conversely, the increasing

of Cu by a factor of ca. 1.5 (Cu−SA7 and Cu−SA9, with 2.00 and 2.63 $atom_{Cu}$ nm^{-2}, respectively) leads to decreasing of the *N* values by a factor of 1.5. Then, the same comparison for Cu−SA9 and Cu−SA12 leads to a higher decreasing of *N* values (1.9) for an increasing of Cu by a 1.4 factor. This observation points out that the increased Cu deposition can play an active role producing catalysts ever more active up to a definite amount (coincident with Cu−SA7 catalyst). Once attained this point, further increasing of Cu deposition on SA did not have any positive effect on the catalyst activity.

The actual evidence confirms our previous findings obtained on copper-based catalysts on crystalline structures[17,44,45] as well as literature findings,[10,12,46,47] that small CuO_x centers well dispersed over supports are more active toward NO_x reduction than large ones. The rather similar catalytic behavior in terms of NO_x conversion to N_2, in particular comparing the specific reaction rates or turnover frequencies, when possible, of Cu−ZSM-5, Cu/Al_2O_3, or Cu/ZrO_2, considering the results obtained from literature,[9,12] and of our CuO-based catalysts supported on acidic silica−alumina, suggests that CuO nanodomains are the common phase in the different samples and that zeolite exchanged copper species or oxo-complexes do not play an exclusive role in the SCR reaction mechanism. Formation of structured aggregates as CuO-like phase led to more silent SCR activity. This is the case for the CuO/SiO_2 system,[12,17] on which the bad dispersion of CuO is related to the absence of an acidic support, and the essential role of acid sites on formation of CuO-active phase and on activity cannot be ruled out.

Results obtained from this investigation points out to individuate an optimum tailoring of the copper particles suitable for SCR process. Too low isolated and dispersed CuO_x species have low turnover numbers, while CuO_x species that are present over surface with density around 1.5−1.7 $atom_{Cu}$ nm^{-2} have the correct tailoring to be catalytically active in the SCR process.

Conclusions

Chemisorption−hydrolysis has been revealed an adequate method to prepare nanodispersed copper catalysts supported over oxidic acidic support. The high surface area of $SiO_2-Al_2O_3$ used as support allows the dispersion of high copper content with uniform spreading of the CuO_x particles. The preparation method avoided the formation of large CuO_x aggregates even when heavy copper loading was deposited on the support. HC-SCR activity depends on copper concentration, maximum activity was associated with 1.5−2 $atom_{Cu}$ nm^{-2}, while for higher copper content the activity and selectivity decreased. This suggests that HC-SCR is a structure-sensitive reaction that is primarily affected by the nature of the active centers and not by the nature of the support, as far as copper dispersion is concerned. Moreover, the nature and dispersion of Cu centers are governed by the acidity of the supports. In this sense, supports even with different structure and composition that are able to nanodisperse the CuO-phase can lead to active SCR catalysts. This conclusion corroborates our previously results[17] as well as literature findings[11,19] on various copper-based catalysts differently supported on modified silica ($SiO_2-Al_2O_3$, SiO_2-TiO_2, and SiO_2-ZrO_2) or alumina supports.

Acknowledgment. This work was carried out with the financial support of MURST (Rome), COFIN2000 − Project "Nitrogen oxides abatement in gaseous emissions with oxides based catalysts", coordinator V. Indovina.

References and Notes

(1) Bosch, H.; Janssen, F. *Catal. Today* **1988**, *2*, 369.
(2) Koebel, M.; Elsener, M.; Kleemann, M. *Catal. Today* **2000**, *59*, 335.
(3) Fridell, E.; Skoglundh, M.; Westerberg, B.; Johanson, S.; Smedler, G. *J. Catal*. **1999**, *183*, 196.
(4) Shelef, M. *Chem. Rev.* **1995**, *95*, 209.
(5) Walker, A. P. *Catal. Today* **1995**, *26*, 107.
(6) Amiridis, M. D.; Zhang, T.; Ferrauto, R. J. *Appl. Catal., B: Environ.* **1996**, *10*, 203.
(7) Misono, M. *CATTECH* **1998**, *2*, 183.
(8) Yahiro, H.; Iwamoto, M. *Appl. Catal., A: Gen.* **2001**, *222*, 163.
(9) Pietrogiacomi, D.; Sannino, D.; Tuti, S.; Ciambelli, P.; Indovina, V.; Occhiuzzi, M.; Pepe, F. *Appl. Catal., B: Environ.* **1999**, *21*, 141.
(10) Chajar, Z.; Primet, M.; Praliaud, H. *J. Catal.* **1998**, *180*, 279.
(11) Bethke, K. A.; Kung, M. C.; Yang, B.; Shah, M.; Alt, D.; Li, C.; Kung, H. H. *Catal. Today* **1995**, *169*, 26.
(12) Márquez-Alvarez, C.; Rodríguez-Ramos, I.; Guerrero-Ruiz, A.; Haller, G. L.; Fernández-García, M. *J. Am. Chem. Soc.* **1997**, *119*, 2905.
(13) Chen, L.; Horiuchi, T.; Osaki, T.; Mori, T. *Appl. Catal., B: Environ.* **1999**, *23*, 259.
(14) Fernandez-Garcia, M.; Rodriguez-Ramos, I.; Ferreira-Apparicio, P.; Guerrero-Ruiz, A. *J. Catal.* **1998**, *178*, 253.
(15) Boccuzzi, F.; Chiorino, A.; Martra, G.; Gargano, M.; Ravasio, N.; Carrozzini, B. *J. Catal.* **1997**, *165*, 129.
(16) Boccuzzi, F.; Coluccia, S.; Martra, G.; Ravasio, N. *J. Catal*. **1999**, *184*, 316.
(17) Carniti, P.; Gervasini, A.; Modica, V. H., Ravasio, N. *Appl. Catal., B: Environ.* **2000**, *28*, 175.
(18) Scofield, J. H. *J. Elect. Spectrosc. Relat. Phenom*. **1976**, *8*, 129.
(19) Fadoni, M.; Lucarelli, L. *Studies in Surface Science and Catalysis*, Adsorption and its applications in industry and environmental protection; Dabrowski, A., Ed.; Elsevier Science Publishers B. V. Amsterdam, 1999; Vol. 120(A), p 177.
(20) Malet, P.; Caballero, A. *J. Chem. Soc., Faraday Trans. 1* **1988**, *84*, 2369.
(21) Monti, D. A. M.; Baiker, A. *J. Catal*. **1983**, *83*, 323.
(22) Cant, N. W.; Cowan, A. D. *Catal. Today* **1997**, *35*, 89.
(23) Auroux, A.; Sprinceana, D.; Gervasini, A. *J. Catal.* **2000**, *195*, 140.
(24) Beutel, T.; Adelman, B.; Sachtler, W. M. H. *Catal. Lett.* **1996**, *37*, 125.
(25) Wu, J.; Larsen, S. C. *J. Catal.* **1999**, *182*, 244.
(26) Gervasini, A., unpublished results.
(27) Beutel, T.; Sárkány, J.; Lei, G.-D.; Yan, J. Y.; Sachtler, W. M. H. *J. Phys. Chem.* **1996**, *100*, 845.
(28) Schneider, P. *Appl. Catal., A: Gen.* **1995**, *129*, 157.
(29) Indovina, V.; Occhiuzzi, M.; Pietrogiacomi, D.; Tuti, S. *J. Phys. Chem. B* **1999**, *103*, 9967.
(30) Dossi, C.; Fusi, A.; Recchia, S.; Psaro, R.; Moretti, G. *Micropor. Mesopor. Mater.* **1999**, *30*, 165.
(31) Schoonheydt, A. *Catal. Rev. Sci. Eng.* **1993**, *35*, 129.
(32) Okamoto, Y.; Gotoh, H.; Aritani, H.; Tanaka, T.; Yashida, S. *J. Chem. Soc., Faraday Trans.* **1997**, *93*, 3879.
(33) Morterra, C.; Giamello, E.; Cerrato, G.; Centi, G.; Perathoner, S. **1998**, *179*, 111.
(34) Shimokawabe, M.; Asakawa, H.; Takezawa, N. *Appl. Catal*. **1990**, *59*, 45.
(35) Friedman, R. M.; Freemam, J. J.; Lytle, F. W. *J. Catal.* **1978**, *55*, 10.
(36) Xu, B.; Dong, L.; Chen, Y. *J. Chem. Soc., Faraday Trans.* **1988**, *94*, 1905.
(37) Córdoba, G.; Viniegra, M.; Fierro, J. L. G.; Padilla, J.; Arroyo, R. *J. Solid State Chem.* **1998**, *138*, 1.
(38) Espinós, J. P.; Morales, J.; Barranco, A.; Caballero, A.; Holgado, J. P.; González-Elipe, A. R. *J. Phys. Chem.* **2002**, *106*, 6291.
(39) Auroux, A.; Gervasini, A.; Guimon, C. *J. Phys. Chem. B* **1999**, *103*, 7195.
(40) Fierro, G.; Lo Jacono, M.; Inversi, M.; Porta, P.; Lavecchia R.; Cioci, F. *J. Catal*. **1994**, *148*, 709.
(41) Bulánek, R.; Wichterlová, B.; Sobalík, Z.; Tichy, J. *Appl. Catal., B: Environ.* **2001**, *31*, 13.
(42) Carniti, P.; Gervasini, A. *React. Kinet. Catal. Lett.* **1999**, *67*, 233.
(43) Gervasini, A.; Carniti, P.; Ragaini, V. *Appl. Catal., B: Environ.* **1999**, *22*, 201.
(44) Gervasini, A.; Picciau, C.; Auroux, A. *Micropor. Mesopor. Mater.* **2000**, *35*, 457.
(45) Carniti, P.; Gervasini, A.; Auroux, A. *Langmuir* **2001**, *17*, 6938.
(46) Torre-Abreu, C.; Ribeiro, M. F.; Henriques, C.; Ribeiro, F. R. *Appl. Catal., B: Environ.* **1997**, *11*, 383.
(47) Praliaud, H.; Mikhailenko, S.; Chajar, Z.; Primet, M. *Appl. Catal., B: Environ.* **1998**, *16*, 359.